Coarse Image Edge Detection using Self-adjusting Resistive-fuse Networks

Haichao Liang and Takashi Morie

Graduate School of Life Science and Systems Engineering, Kyushu Institute of Technology
Kitakyushu, Fukuoka, 808-0196, Japan

Abstract. We propose a model of coarse edge detection using self-adjusting resistive-fuse networks. The resistive-fuse network model is known as a nonlinear image processing model, which can detect coarse edges from images by smoothing noise and small regions. However, this model is hardly used in real environment because of the sensitive dependence on the parameters and the complexity of the annealing process. In this paper, we first introduce self-adjusting parameters to reduce the number of parameters to be controlled. Then, we propose a heating-and-cooling sequence for fast and robust edge detection. The proposed model can detect edges more correctly than the original one, even if an input image includes a gradation.

1 Introduction

Edge detection is a common task in image processing. It can not only serve for pattern recognition, such as image retrieval [1] and text extraction [2], but can also reduce the image information to accelerate conventional image processing [3, 4].

In some applications, coarse edge detection is desired to reduce the complexity of edge images. The resistive-fuse network model provides such a function [5]. This model smoothes image noise and small regions, and detects discontinuities as coarse edges by using iterative operations to minimize an energy function. This model can converge faster than stochastic methods [6] or coupled MRF models [7]. Therefore, we have used this model for coarse edge detection and have implemented it in an FPGA [8].

However, the resistive-fuse network model has two limitations: sensitive dependence on the parameters, and complexity of the annealing process, which is necessary to avoid local minimum. These two limitations greatly restrict the use of this model in real applications.

In this paper, we propose a new resistive-fuse network model. We first introduce a self-adjusting element to reduce the number of parameters to be controlled. Then, we propose a new annealing sequence for fast and robust edge detection.

2 Original Resistive-fuse Network Model

Resistive-fuse networks (hereafter, RFN) are used to implement an image reconstruction model, which performs energy minimization for coarse edge detection [5]. The energy function is given by

Liang H. and Morie T.
Coarse Image Edge Detection using Self-adjusting Resistive-fuse Networks.
DOI: 10.5220/0003015600430052
In *Proceedings of the 10th International Workshop on Pattern Recognition in Information Systems (ICEIS 2010)*, page
ISBN: 978-989-8425-14-0

$$E(f) = \sigma \sum_i (f_i - d_i)^2 + \lambda \sum_i (f_i - f_{i+1})^2 (1 - l_i) + \alpha \sum_i l_i, \tag{1}$$

where f_i, d_i and l_i are the values of the pixel state f, input data d and binary line processes l at location i, respectively, and σ, λ and α are free parameters. The first term forces the pixel state f to be close to the input data d, while the second term smoothes that. The third term, line processes l, functions as follows.

$$l_i = \begin{cases} 1, & \lambda(f_i - f_{i+1})^2 > \alpha, \\ 0, & otherwise. \end{cases} \tag{2}$$

So far, many methods have been proposed to solve the local minimum problem in an MRF model, such as stochastic methods or using coupled MRF model. However, a continuation method, such as the graduated non-convexity (GNC) algorithm [9], can make the model converge fast and is therefore suitable for real-time image processing. Such an method eliminates the line processes l, and gradually changes the energy function from a convex shape to the final desirable one.

RFN circuit implements the model using the continuation method. The original RFN circuit is composed of voltage sources, linear resistances and resistive-fuse elements, as shown in Fig. 1 (a). Each node corresponds to a pixel state $f_{i,j}$, when the value of each voltage source represents the image input $d_{i,j}$ at pixel (i, j). Each node and voltage source are connected with a linear resistance, whose conductance is σ. The adjacent nodes are connected with resistive-fuse elements, whose conductance function is given by

$$I = G(V) = \frac{\lambda V}{1 + \exp\{\eta(V^2 - \delta^2)\}}, \tag{3}$$

where λ is the conductance of a resistive-fuse, η is a parameter for changing the conductance function, and δ is the threshold value of the resistive-fuse elements. Equation (3) is derived by using a deterministic mean field approximation to the MRF model of piecewise smooth surface interpolation [10], and the parameter η in this equation corresponds to the inverse of the *temperature* T for simulated annealing [6].

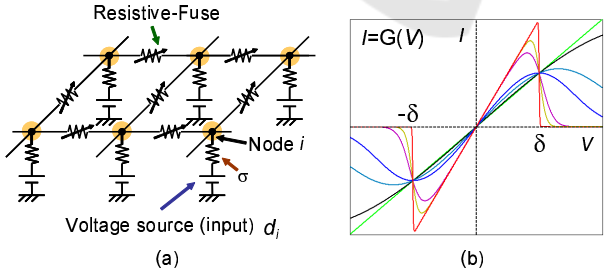

Fig. 1. Original analog resistive-fuse network (a), and I-V characteristics (b) of a resistive-fuse element.

The energy function of this circuit is given by

$$E(f) = \sigma \sum_{i,j} (f_{i,j} - d_{i,j})^2 + \sum_{i,j} \sum_{m,n \in N} \int_0^V G(v) dv, \tag{4}$$

where N represents the neighboring nodes of (i, j), and $V = f_{i,j} - f_{m,n}$.

When η is close to zero, i.e. temperature T is very high, the conductance is almost linear, as shown in green color in Fig. 1 (b). In contrast, when η is equal to or larger than unity, i.e. temperature T is very low, the conductance becomes an ideal resistive-fuse characteristic, which is similar to the line process function, as shown in red color in Fig. 1 (b).

As described above, the original RFN model uses a continuation method to avoid the local minimum problem, by gradually changing the parameter η from near zero to unity or larger than that. This is based on the assumption that the unique minimum of the convex energy function is close to the global minimum of the final function shape.

In practice, we calculate the pixel state *f* by using discrete-time dynamics with an equation derived from the Kirchhoff's Current Law (KCL). The dynamics is given by

$$f_{i,j}(t+1) = f_{i,j}(t) - \xi\{ \sum_{m,n \in N} G(V) + 2\sigma(f_{i,j} - d_{i,j})\}, \tag{5}$$

where ξ is a step size parameter of gradient descent. The change of η is called an *annealing* process, and the annealing schedule is usually as follows:

$$\eta(t+1) = k\eta(t), \tag{6}$$

where t is the index of iterations, and k is a real number which fulfills $k \in (1, 2]$ [6, 9].

3 Limitations of Original RFN Model

The RFN model mainly has two limitations in actual applications, and each of them is described in a following subsection.

3.1 Dependence on the Parameters

The original RFN model has four parameters for controlling the energy function: λ, σ, η and δ. Each of them affects the results of edge detection. λ and σ control the strength of smoothing, while η and δ control the range of that, i.e. the balance of smoothing and segmentation. Therefore, it is necessary to make clear the relationships between these parameters for the control of them.

First of all, let us focus our attention on the relationship between λ and σ. It is obvious that the value of λ/σ determines the constraint of the input image and the strength of smoothing. Therefore, the results of edge detection not only depend on the threshold δ, but also sensitively depend on λ/σ, as shown in Fig. 2 (a). The larger the ratio is, the stronger the strength of smoothing becomes.

Next, we discuss the relationship between η and δ. It is verified from Fig. 2 (b) that the shapes of the energy function and conductance function $G(\cdot)$ vary according to both η and δ. This means that the balance of smoothing and segmentation will vary accordingly when using the same annealing schedule and different δ. This makes it difficult to select the threshold δ.

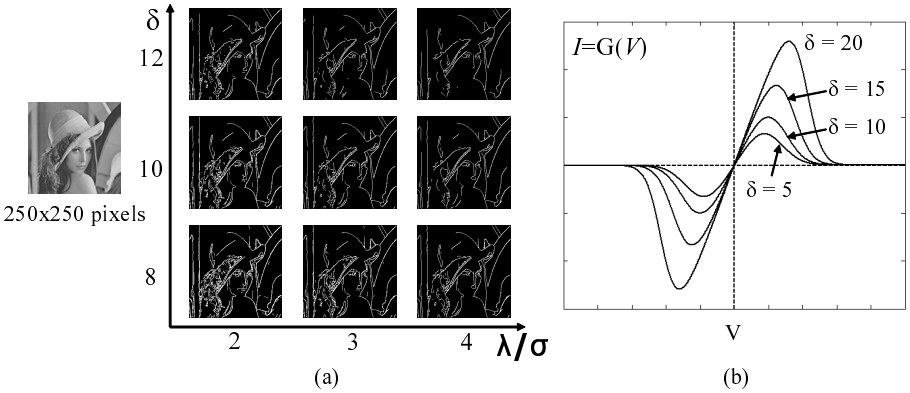

Fig. 2. (a) Edge detection results using RFN model, when $\eta(0)$ = 0.00055, k = 1.1 and iterations = 80 in Eq. (6), and (b) Variations of the shape of conductance function, when $\eta = 0.01$.

3.2 Complexity of Annealing Process

We use a simple circuit as shown in Fig. 3 (a) to discuss the annealing process. In this case, the energy function is given by

$$E(f) = \sigma(f_i - d_i)^2 + \int_0^{V_i} G(v)dv + \sigma(f_{i+1} - d_{i+1})^2 + \int_0^{-V_i} G(v)dv, \quad (7)$$

where $V_i = f_i - f_{i+1}$.

When the energy function $E(f)$ reaches a minimum, we can obtain the following equations:

$$\frac{\partial E}{\partial f_i} = 2\{\sigma(f_i - d_i) + G(V_i)\} = 0. \quad (8)$$

$$\frac{\partial E}{\partial f_{i+1}} = 2\{\sigma(f_{i+1} - d_{i+1}) + G(-V_i)\} = 0. \quad (9)$$

These two equations mean that E_f reaches a minimum when the sum of the currents at each node is zero, i.e. the circuit is in a stable state. Subtracting Eq. (9) from Eq. (8) gives

$$G(V_i) = \sigma\frac{V_{ddi} - V_i}{2}, \quad (10)$$

where $V_{ddi} = d_i - d_{i+1}$. The right-hand side of Eq. (10) is therefore identical to the current in the linear resistance between f_i and d_i. In Fig. 3 (b), the black lines and the red lines represent I_{Ri} ($\eta = 1$) and I_{ri}, where I_{Ri} and I_{ri} denote the left-hand and right-hand side of Eq. (10), respectively. It is clear that I_{ri} follows a linear function of V_i because V_{ddi} is given by the input. Therefore, the intersection points of them represent the stable states of the circuit.

Figure 3 (b) and Table 1 show that the number of stable states depends on the value of V_{ddi}, which is the intersection point of the red lines and the V_i-axis. There is only one

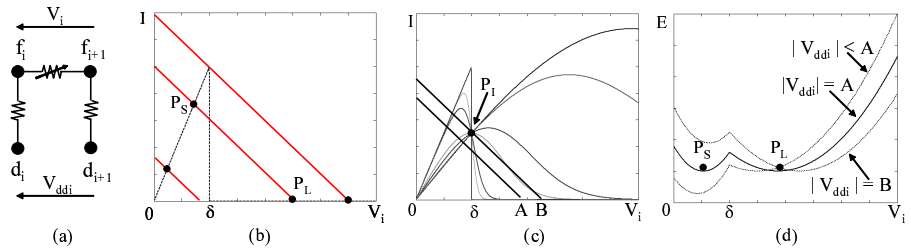

Fig. 3. A simple circuit (a) for discussion, and the relationship (b) between I_i and V_i where $V_i = f_i - f_{i+1}$. (c) and (d) show the definitions of *A* and *B* using relationship between I_i and V_i and that between P_S and P_L ($\eta = 1$), respectively.

Table 1. Local minimum problem concerned with v.

Value of $\lvert V_{ddi}\rvert$	E_{min}	G	U	Definitions	
$\lvert V_{ddi}\rvert \in (0, \delta)$	single	Region S	Region S	A = $\delta\sqrt{1+\frac{2\lambda}{\sigma}}$, B = $\delta(1+\frac{\lambda}{\sigma})$, C = $\delta(1+\frac{2\lambda}{\sigma})$	
$\lvert V_{ddi}\rvert \in (\delta, A)$	multiple	Region S	Region S	G	Global E_{min} when $\eta \geqq 1$
$\lvert V_{ddi}\rvert \in (A, B)$	multiple	Region L	Region S	U	Unique E_{min} when $\eta \approx 0$
$\lvert V_{ddi}\rvert \in (B, C)$	multiple	Region L	Region L	Region S	the region where $\lvert V_i\rvert < \delta$
$\lvert V_{ddi}\rvert > C$	single	Region L	Region L	Region L	the region where $\lvert V_i\rvert > \delta$

stable state if V_{ddi} is smaller than δ or is large enough. However, there are two stable states, which are denoted by P_S and P_L, if $V_{ddi} \in (A, B)$ where A and B are defined as shown in Fig. 3 and Table 1.

Note that the series of the conductance function intersect at a point $(\delta, \lambda\delta/2)$, which can be calculated from Eq. (3) and is shown as P_I in Fig. 3 (c). Thus, *A*, *B* and *C* in Table 1 are defined as follows:

- If V_{ddi} = A, $E(P_S) = E(P_L)$.
- If V_{ddi} = B, the red line moves across P_I.
- If V_{ddi} = C, the red line moves across $(\delta, \lambda\delta)$.

As described in Sec. 2, the annealing process in RFN model relies on the assumption that the unique minimum of the convex energy function is close to the global minimum of the final desired one at each node. Here, "close" can be defined as in the same region where $\lvert V_i\rvert < \delta$ or $\lvert V_i\rvert > \delta$, i.e. in the region *S* or region *L*.

It is clear from Table 1 that such assumption is not valid when $V_{ddi} \in (A, B)$, which we called a *gray zone*. Note that if $\lvert V_i\rvert > \delta$, the two nodes will be smoothed from the beginning when using an annealing sequence, such as the annealing schedule shown in Eq. (6) or a simplified three-stage sequence proposed in [8]. Because there was no algorithm to prevent the nodes moving into the gray zone, such an annealing sequence can not always give the global minimum solution at each node, and might cause over-smoothing and lose some edges. Therefore, the annealing schedule should be redesigned by considering the relationship between δ, η and λ/σ.

4 Improved RFN Model

In order to improve the RFN model, we first introduce self-adjusting functions of λ and η to reduce the number of parameters to be controlled. Then, we propose a new annealing sequence for fast and robust edge detection.

4.1 Self-adjusting of λ

We first propose a self-adjusting function of λ as shown in Eq. (11), which has the similar effect as the annealing process.

$$\lambda_{m,n}(t+1) = \begin{cases} \lambda_{m,n}(t)(1+h_\lambda), & |V| < \delta, \\ \lambda_{m,n}(t)(1-h_\lambda), & otherwise. \end{cases} \tag{11}$$

Here, h_λ is a small positive number and can be determined by the number of iterations and the range of adjustment.

By using this self-adjusting function of λ, we can set σ and the initial value of λ as constants, and let λ adjust itself to change the value of λ/σ according to the local voltage difference. Thus, the manual control of λ and σ becomes unnecessary. Furthermore, this self-adjusting can also improve the robustness of the model because it can reduce the length of gray zone by decreasing λ/σ when $|V| > \delta$.

4.2 Self-adjusting of η

In order to keep the balance of smoothing and segmentation, we obtain Eq. (12) for the scaling of conductance function when parameters except η and δ remain identical.

$$G_1(V)|_{V=k\delta_1} : G_2(V)|_{V=k\delta_2} = \delta_1 : \delta_2, \tag{12}$$

where k is a certain real number. Thus, we obtain the condition as follows by substituting Eq. (3) into Eq. (12).

$$\eta_1\delta_1^2 = \eta_2\delta_2^2 \tag{13}$$

This means that η can be adjusted by δ and the desired shape of the conductance function.

Summarizing the above, the number of parameters need to be controlled can be reduced to one, i.e. only the threshold δ, by using the self-adjusting functions of λ and η. This result significantly simplifies the control of the parameters, and makes it easier to select the appropriate threshold δ.

4.3 New Annealing Sequence

We propose a heating-and-cooling annealing sequence, and employ a “shaping” process, which is named after that in the die making, to reduce the complexity and ambiguity of the input image for robust edge detection. The details of the proposed annealing sequence are as follows. If the defined threshold value is δ_0,

1. "Sharpening" stage: $\delta = \delta_0/2$ and $\eta = 1$.
2. "Shaping" stage: $\delta = \delta_0$ and $\eta = 1$.
3. "Heating" stage: $\delta = \delta_0$ and $\eta = 0.1/\delta^2$.
4. "Cooling" stage: $\delta = \delta_0$ and $\eta = 5/\delta^2$.

In the first stage, we use a small δ to sharpen blurred boundaries. During this stage, the interactions between two nodes where $|V| > \delta_0/2$ will be cut off and blurred boundaries will be sharpened by the smoothing in a small range.

In the second stage, we set $\delta = \delta_0$ and $\eta = 1$ to calculate the rough results which obviously include the local minimum and small regions.

In the third stage, we use a small η, i.e. high temperature to smooth small regions and to lead to global minimum.

In the final stage, we use a large η, i.e. low temperature to "cool" the pixel states down for coarse edge detection. Note that η is a little smaller than unity in the final stage. This is because that the binary resistive-fuse characteristic is known as lack of robustness [11]. Therefore, we use $\eta = 5/\delta^2$ in the final stage, whose characteristic is close to that when $\eta = 1$, but more convex around where $|V| = \delta$. Therefore, it may lead to less local minimum in the interactions with neighboring eight nodes.

In summary, we propose a heating-and-cooling annealing sequence, and employ "sharpening" and "shaping" processes to improve the robustness of the model. Ideal annealing sequences have to smooth noise and small regions at the same time, while keeping the boundaries of large regions. However, simple cooling-down annealing cannot achieve these functions due to the uncertainty of the input image, and may cause oversmoothing. In contrast, the proposed annealing sequence can sharpen blurred boundaries and reduce noise in the input image before the "heating" stage for smoothing the small regions. Therefore, the proposed annealing sequence can achieve more robust detection than simple cooling-down sequences.

5 Simulation Results and Discussion

Figure 4 (a) shows processing results obtained by applying the self-adjusting function of λ to the original RFN model. It is verified that these results are less sensitive to the initial value of λ/σ compared with Fig. 2 (a). Figure 4 (b) shows the scaling of the shape of conductance function, by keeping $\eta\delta^2$ constant.

We also evaluated the similarity between the results where (initial value of) λ/σ is two and is four as shown in Table 2. The similarity is defined as the ratio of the count of identical edge pixels to that of all the edge pixels. In the simulation, 15 images are selected from 4.1.01 to 4.2.07 in the USC-SIPI Image Database [12]. By comparing 3rd-column with 4th-column in Table 2, it is verified that our self-adjusting function can significantly weaken the dependence of the model on λ/σ, so that it can increase the similarities of edge detection results when changing λ/σ. Furthermore, the similarities of edge detection results come to more than 90% by additionally using our new annealing sequence as shown in the 5th-column in Table 2. Therefore, the manual control of λ and σ is unnecessary any more.

Figure 5 shows processing results for images with gradation. The rectangular region in the input image has a gradation of 10 levels per pixel in 256-level grayscale. These

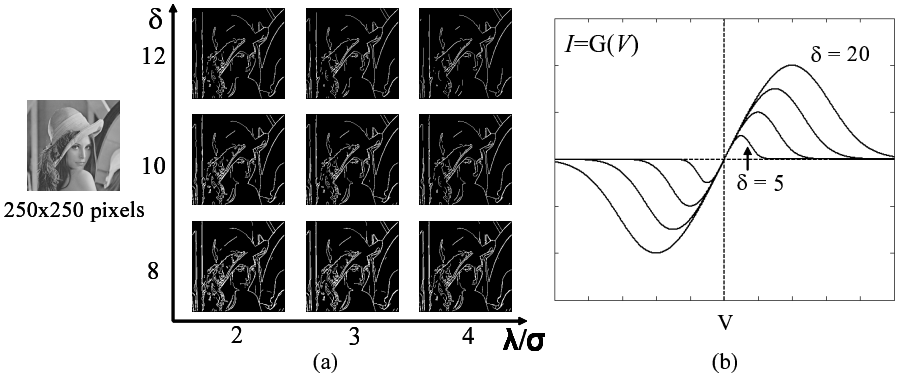

Fig. 4. (a) Edge detection results using self-adjusting of λ. The horizontal axis represents the initial value of λ/σ. (b) Scaling of the shape of conductance function $G(\cdot)$, by using $\eta\delta^2 = 1$.

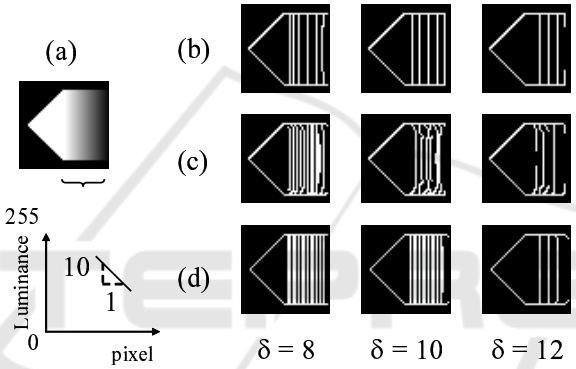

Fig. 5. Edge detection results in the case of gradation. Input image (a) with a gradation, and edge detection results using original RFN model (b), a simplified RFN model (c) in [8] using a three-stage-cooling annealing sequence, and our proposed RFN model (d).

Table 2. Similarity Evaluation of Edge Detection Results.

	δ	Original model	Adjusting of λ only	Proposed model
Lena	12	55.09%	69.13%	91.44%
	10	58.14%	74.36%	93.32%
	8	56.46%	77.59%	93.64%
Average	12	56.65%	69.43%	92.94%
	10	57.41%	73.85%	93.61%
	8	57.12%	75.67%	94.18%

results show that the original RFN model with an annealing process described in Eq. (6) can only detect coarse edges, and the model with a simplified three-stage-cooling annealing sequence [8] failed to detect correct edges in the gradation region. In contrast, the proposed model in this paper can detect coarse edges when $\delta > 10$, and can detect fine edges when $\delta \leq 10$.

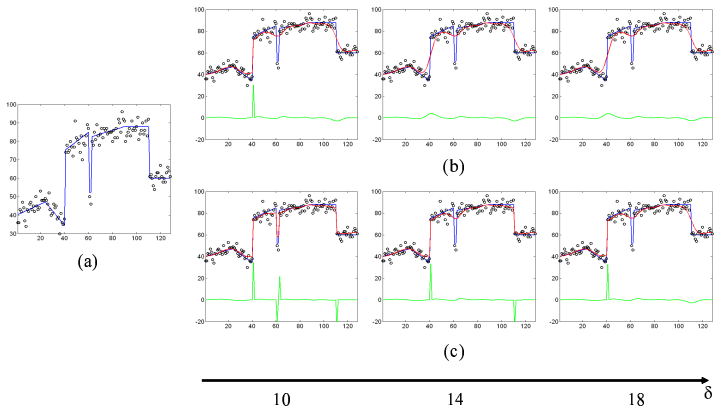

Fig. 6. Edge detection results using one-dimension input data with Gaussian white noise. Input data (a), and edge detection results using original RFN model (b) and proposed model (c). Here, red color shows the pixel state, and green color shows the first derivation of that.

Figure 6 shows some results using input data shown in black color in Fig. 6 (a), which is obtained by adding Gaussian white noise (sigma = 4) to the data shown in blue color. In this simulation, λ/σ in the original RFN model and its initial value in the proposed model were set to three. It is verified that original RFN model can detect almost no edges because the boundaries are over-smoothed, as shown in Fig. 6 (b). In contrast, the proposed model can control the level of edge detection, as shown in Fig. 6 (c), when $\lambda_{min} = 2$ and $\lambda_{max} = 4$.

6 Conclusions

We analyzed the resistive-fuse network model for coarse edge detection and clarified its limitations. First, we proposed self-adjusting functions to simplify the parameter control. We concluded that only the threshold δ has to be controlled, and the local-adjusting of λ improves the robustness of edge detection. Then, we proposed a new annealing sequence for fast and robust detection. It was verified that the proposed model can detect edges more correctly than the original one, even if an input image includes a gradation.

Acknowledgements

This work was partly supported by fund from MEXT, Japan, via a Knowledge Cluster Initiative Second Stage program, granted to Fukuoka Cluster for Advanced System LSI Technology Development.

References

1. Phan, R., Androutsos, D.: Content-based retrieval of logo and trademarks in unconstrained color image databases using color edge gradient co-occurrence histograms. Computer Vision and Image Understanding 114 (2010) 66–84
2. Tsai, T. H., Chen, Y. C., Fang, C. L.: 2DVTE: A two-directional videotext extractor for rapid and elaborate design. Pattern Recognition 42 (2009) 1496–1510
3. Toulminet, G., Bertozzi, M., Mousset, S., Bensrhair, A., Broggi, A.: Vehicle detection by means of stereo vision-based obstacles features extraction and monocular pattern analysis. IEEE Trans. on Image Processing 15 (2006) 2364–2375
4. Naito, T., Ito, T., Kaneda, Y.: The obstacle detection method using optical flow estimation at the edge image. In: IEEE Intelligent Vehicles Symposium, Istanbul, Turkey (2007) 817–822
5. Harris, J. G., Koch, C., Staats, E., Luo, J.: Analog hardware for detecting discontinuities in early vision. Int. Journal of Computer Vision 4 (1990) 211–223
6. Geman, S., Geman, D.: Stochastic relaxation, Gibbs distributions, and the Bayesian restoration of images. IEEE Trans. on Pattern Analysis and Machine Intelligence 6 (1984) 721–741
7. Kawashima, Y., Atuti, D., Nakada, K., Okada, M., Morie, T.: Coarse image region segmentation using region- and boundary-based coupled MRF models and their PWM VLSI implementation. In: Int. Joint Conf. on Neural Networks (IJCNN2009), Atlanta, USA (2009) 1559–1565
8. Nakano, T., Morie, T., Ishizu, H., Ando, H., Iwata, A.: FPGA implementation of resistive-fuse networks for coarse image-region segmentation. Intelligent Automation and Soft Computing 12 (2006) 307–316
9. Blake, A.: Comparison of the efficiency of deterministic and stochastic algorithms for visual reconstruction. IEEE Trans. on Pattern Analysis and Machine Intelligence 11 (1989) 2–12
10. Geiger, D., Girosi, F.: Parallel and deterministic algorithms from MRF's: Surface reconstruction. IEEE Trans. on Pattern Analysis and Machine Intelligence 13 (1991) 401–412
11. Harris, J.G.: Analog models for early vision. PhD thesis, California Institute of Technology (1991)
12. (USC-SIPI) http://sipi.usc.edu/database/.